



Contents lists available at ScienceDirect

International Journal of Thermal Sciences

journal homepage: www.elsevier.com/locate/ijts

Effect of nanoparticles on condensation of humid air in vertical channels

Iman Zeynali Famileh ^{a, b}, Javad Abolfazli Esfahani ^a, Kambiz Vafai ^{b, *}

^a Center of Excellence on Modeling and Control Systems, (CEMCS) & Department of Mechanical Engineering, Faculty of Eng., Ferdowsi University of Mashhad, Iran

^b Mechanical Engineering Department, University of California, Riverside, CA, USA

ARTICLE INFO

Article history:

Received 22 February 2016

Received in revised form

8 May 2016

Accepted 8 May 2016

Available online xxx

Keywords:

Filmwise condensation

Non-condensable gas

Nano-particles

Humid air

Heat and mass transfer

ABSTRACT

In this paper, the effect of uniform surface injection of nanoparticles on humid air condensation, as a main type of vapor condensation in the presence of non-condensable gas (NCG), is numerically investigated. Various inlet conditions (velocity and relative humidity) of vertical CONAN type classical test section were modeled. Two mass concentrations of different nanoparticles were examined and the behavior of filmwise condensation was studied under different parameters of heat and mass transfer, such as: Reynolds number and mean Nusselt number of the condensed film, and local and mean Sherwood number. Finally, by using response surface methodology, the statistical interpretation (objective function) of the numerical results are provided for other inlet conditions. As shown in the results, an increase in the nanoparticles mass concentration has direct influence on condensate Reynolds number and Sherwood number of the humid air. At higher relative humidities (ω), using nanoparticles has more impact and the maximum improvement of the condensate Reynolds number (at the outlet), mean Nusselt number of the condensed film and mean Sherwood number are 11.4, 4.5 and 6%, respectively. It is observed that, under best conditions ($\omega = 100\%$, $U_{in} = 3$ m/s), 0.5% of nanoparticles mass concentration improves the total heat flux by more than 10.4%.

© 2016 Elsevier Masson SAS. All rights reserved.

1. Introduction

The humid air condensation, as an example of condensation in the presence of NCG, is one of the most applicable methods of phase change which is observed in different industrial equipment such as Heating, Ventilating and Air Conditioning (HVAC) or coolant systems. For this purpose, various studies focused on filmwise condensation enhancement with multifarious passive or active methods. Undeniably, transformation to the era of nano-technology has a strong potential for improvement of phase change performance. Therefore, using nano-material, as an additive to the main fluid, is considered and several investigators have tried to evaluate the effect of nano-materials on heat and mass transfer enhancement in heat exchangers [1–3]. Accordingly, a better understanding of the nano-particles/nano-fluids effects on heat and mass transfer, especially in the presence of phase change, and its influence on the mechanism of condensation/evaporation is

needed as a key factor for more efficient equipment design.

1.1. Condensation of humid air

There are comprehensive studies in the area of filmwise condensation for pure vapor and air/vapor mixture, with several correlations for heat and mass transfer parameters for various geometrical conditions [4–6]. Desrayaud and Lauriat [7] demonstrated a new analogy of heat and mass transfer for condensation of humid air under laminar natural convection flow. Based on the thin film assumption, they reported new correlations for Sherwood number, latent and sensible Nusselt numbers. Rao et al. [8] performed an analytical model for laminar film condensation of vapor in the presence of air as a high concentration of NCG in a vertical tube. With the help of heat and mass balance equations at the interface, they estimated the gas-liquid interface temperature and reported the condensate Nusselt number, condensate Reynolds number and pressure drop for different inlet conditions, such as Reynolds number in the range of 1000–2000, and relative humidity up to 80%. In a similar study, Wu and Vierow [9] investigated the condensation of the vapor in the presence of NCG in a

* Corresponding author.

E-mail address: vafai@engr.ucr.edu (K. Vafai).

horizontal tube and compared the condensation heat transfer coefficient at the top and bottom of the tube. By comparing the centerline temperature profiles and the overall heat transfer rate, the global effect of NCG on the heat transfer rate was evaluated and the local effects of NCG on condensation process were reported.

Ambrosini et al. [10,11] attempted to compare the numerical simulation of several CFD commercial software with the experimental benchmark results of the CONAN typical classical test section. The experimental correlations of Nusselt number and Sherwood number for wall condensation of an external flow over a vertical flat plate was proposed by them. Vyskocil et al. [12] carried out air-steam condensation numerically and highlighted the simulation of wall condensation ignoring the effect of volume condensation. They compared their results with the benchmark data of CONAN experimental facility and predicted the condensation rate for different inlet conditions. Similarly, Zschaek et al. [13] provided a new CFD model of the wall condensation of vapor in the presence of non-condensable multi components gas mixture in a vertical channel and compared the numerical results with experimental data of CONAN experimental facility [10]. A comprehensive review of vapor condensation in the presence of NCG was done by Huang et al. [14]. They categorized previous studies into dropwise and filmwise condensation and focused on semi-theoretical and theoretical models of condensation process in the presence of NCG. The effect of condensate thickness film, surface waves, interfacial shear strength and suction effects on filmwise condensation in the presence of NCG were evaluated by them. Saraireh et al. [15] used ANSYS FLUENT commercial CFD software with the aim of comparing the numerical results with well-established correlations of wall condensation parameters (condensation rate of vapor and heat flux) in the presence of air. Agrawal and Das [16] used in-house developed CFD code (HDS) and modeled unsteady form of wall film condensation under hydrogen distribution in an enclosure which is filled with mixture of vapor and air for a vertical injection of hydrogen from the bottom. They claimed that downward motion of the condensed film causes the concentration of hydrogen in lower parts of the enclosure. Szijarto et al. [17] utilized RELAP5, a thermal-hydraulic system code, to trace the wall condensation and provided the prediction of heat transfer process considering variation of temperature, pressure and void fraction of vapor along the horizontal pipe. In their study, based on three different regimes of condensation, they defined the significant role of stratification angle for transient condensation in a horizontal pipe. The numerical models of natural convection and wall condensation of humid air with time dependent wall temperature were defined by Sun et al. [18]. The thickness of the condensed film was discussed and it was claimed that the thickness reflects on the flow structures. The effect of geometrical parameters (such as aspect ratio of cavity) on wall condensation/evaporation was also addressed.

1.2. Nanoparticles application in convection heat transfer

Modeling of the particles behavior in gaseous phase is important for several processes and there are many works in the literature focused on investigation of particle deposition and suspended particle effects on heat transfer. Hudson [19] studied numerically the effect of copper nanoparticles on the enhancement of laminar natural/forced convection regime in a tube and an enclosure with different aspect ratios. Different particles tracking methods for various enclosures, with aspect ratio between 1 and 5, were examined and finally it was concluded that nanoparticles has a tendency to stay near the borders of an enclosure. Brereton [20] developed a Eulerian model for prediction of particle transport in an internal turbulent flow with thermophoretic term, as an eddy-viscosity-scaled multiple of the corresponding mean

thermophoretic term, which is applicable for low inertia particles. Walsh et al. [21] developed an investigation of thermophoretic deposition of aerosol particles on relatively cool cylindrical tube. Based on the solution of aerosol population, they compared particles deposition in downward/upward flow through a vertical pipe and found that the free convection effects could be ignored for lower bulk Richardson number ($Ri < 1$). A two phase Euler-Euler model for prediction of conduction, convection and radiation heat transfer in dense gas-particle domains on the open-source code OpenFOAM for high temperature solar power applications was provided by Marti et al. [22]. In case of a moderate rise in the wall temperature (581 K) and particle diameter of 64 μm , they highlighted that the solid conduction accounts for about 97% of the wall to suspension heat flux. The increase of radiation heat flux portion up to 10% of the total wall to suspension heat flux is reported by them.

In order to evaluate particles force balance, Akbar et al. [23] studied the transport of particles in a square enclosure for laminar free convection regime using Eulerian-Lagrangian method at ANSYS FLUENT commercial CFD software. They investigated different motion mechanisms, including gravity, drag and lift forces, and thermophoresis and Brownian dispersions, for different Rayleigh numbers ranging from 100 to 800,000 and found that most of the particles dispersed towards the walls, while a portion of the particles were collected in a quasi-steady recirculation zone. Garoosi et al. [24], used Eulerian-Lagrangian hybrid method, to model deposition of solid particles in natural convection regime of an insulated square cavity with different replacement of cooler and heater elements. Tracking of 6000 discrete particles within a range of Rayleigh numbers ($10^4 \leq Ra \leq 10^7$) showed that thermophoresis force could be effective at lower Rayleigh numbers. For the case which were studied, at lower Rayleigh numbers and non-uniform distribution of particles; using more coolers and splitting elements into smaller segments causes a significant change in deposition rate of particles and heat transfer rate. Afshar et al. [25] solved the Navier-Stokes and energy equations for slip flow regime in microchannel analytically and evaluated dispersion of particles due to the mentioned effective parameters. In their analysis, it was shown that the control of entrance location of nanoparticles leads to a heat transfer enhancement. Additionally, a decrease in the particle diameter causes an increase in the surface to volume fraction, which is affects, the heat transfer in microchannels. In order to compare Eulerian and Lagrangian approaches, Saidi et al. [26] compared the motion of particles for the same problem using the two cited approaches. Their overall results showed that for low particles concentration, approximately 10^5 m^{-2} , the Eulerian approach diverges considerably and cannot be applicable for low particles concentration unless employing a long time scale. Using numerical solution of similarity transformations, Alam et al. [27] investigated unsteady forced convection heat and mass transfer equations for thermophoretic deposition of micro-particles driven by a rotating disk. Axial thermophoretic velocity, thermophoretic deposition flux and concentration profiles of particles were evaluated at different Schmidt number and it was concluded that, for larger Lewis numbers, the increasing trend of thermophoretic velocity could be affected by thermophoretic coefficient and thermophoresis parameter.

Based on general exact solution of particle transport [28], Bertoli et al. [29] obtained several limiting solutions for heat transfer in multi-particles systems, single particle and single phase flow. The effect of magneto hydrodynamic (MHD) on transportation and deposition of micro- and nano-sized particles (particle diameter in the range of 1 nm to 1 μm) for natural convection regime over a horizontal and vertical plate was proposed by Guha and Samanta [30,31]. Different parameters such as: free convection, Brownian

diffusion and thermophoresis effects were included and particles concentration and deposition velocity of particles for different magnetic field parameters were reported. It was shown that the magnetic field parameter decreases the deposition velocity with an increase in the particle diameter. The particle deposition at the bottom surface in room scale chamber with point particles injection from two wall sides was numerically presented by Zhang et al. [32]. Distribution of particle-number density (count/volume) under different situations was evaluated and the best agreement between the modeling and the experiments was achieved for intermediate particles size range (around 30 μm). With similar aim, Wang et al. [33] used ANSYS FLUENT commercial software and modeled particles prediction in an airliner cabin for seven particle sizes (in the range of 0.1–100 μm). They tried to find the most important factor in particle deposition and provided an estimation of the position of particle concentrations.

Although the effects of nanoparticles on heat transfer, especially convection and radiation, were considered in recent studies, there is no comprehensive study in the area of nanoparticles deposition effects on phase change (condensation). In the present study, the effect of nanoparticles on filmwise condensation of vapor in the presence of large volume of air, as a NCG, for different inlet velocities and relative humidities of vertical channel are investigated and local and mean values of heat and mass transfer parameters are discussed. This investigation is divided in three different parts. In the first part, the effect of nanoparticles material and mass concentration of nanoparticles are evaluated. In the second part, condensate Reynolds number, Nusselt number of the condensed film and Sherwood number are investigated. In the third part, based on the response of surface methodology (RSM) the objective function of the investigated parameters of the present problem were provided. Finally, using the provided correlation, the influence of nanoparticles for various ranges of relative humidity and inlet velocity are investigated. Due to the small effect of nanoparticles on the condensed film, the variation of condensed film specifications is not large. However, because of the presence of particles in different applications of humid air condensation, the investigation of these effects are significant and prediction of the exact trend of filmwise condensation in the mentioned conditions is appreciable. Therefore, the investigation of nanoparticles effects on condensation of vapor in the presence of air is the aim of present research.

2. Problem statement

Fig. 1 displays the schematic view of the CONAN typical classical test section (a vertical channel with the cooling system in one side and three insulated walls). The uniform dilute gas-particle flow (a multiphase system of nanoparticles as a discrete phase and humid air) enter from the above and exit from the below side. It was assumed that the nanoparticles were injected from an inlet surface uniformly and with similar hydrodynamic and thermal conditions of the main stream. The coolant water at fixed mass flux and inlet temperature flows from below to a thin secondary channel on the other side of the cooling wall. This situation causes the condensation of the vapor on the coolant wall of the main channel and because of the gravity force, as the only external body force, the condensed film has a downward movement along the cooling wall and the exit from below.

As mentioned before, the aim of this paper is the investigation of nano-particle effect on the condensation and, for this purpose; it is preferred to select the condition with minimum convection and radiation heat flux between the main stream and the cooling wall. That is, under the considered conditions where the condensed vapor takes the form of filmwise condensation, the condensation

heat flux is greater than convection heat flux (This assumption is prepared in CONAN typical classical test section.) [34]. Therefore, there are several limitations for the inlet boundary, which causes filmwise condensed flow. What is more, because of the low temperature main stream (a multiphase system of nanoparticles as a discrete phase and humid air), the radiation heat transfer can be ignored [35]. Accordingly, the effect of nanoparticles on filmwise condensation can be investigated under the mentioned geometrical and hydrodynamical specifications of the problem, which are listed in Table 1. The influence of particles deposition is much larger in turbulent flows. As such all of investigated conditions are selected in turbulent regime.

3. Governing equations

For the mentioned process, governing equations such as: continuity, momentum, energy, species transport and particles force balance in vertical form for steady state condition could be written as follows:

Continuity equation:

$$\nabla \cdot (\rho \vec{V}) = 0 \quad (1)$$

Momentum equations:

$$\nabla \cdot (\rho u \vec{V}) = -\frac{\partial p}{\partial x} + \nabla \cdot (\mu_{eff} \nabla u) \quad (2)$$

$$\nabla \cdot (\rho v \vec{V}) = -\frac{\partial p}{\partial y} + \nabla \cdot (\mu_{eff} \nabla v) + \rho g \quad (3)$$

$$\nabla \cdot (\rho w \vec{V}) = -\frac{\partial p}{\partial z} + \nabla \cdot (\mu_{eff} \nabla w) \quad (4)$$

where ρ and \vec{V} are the density of humid air and the velocity vector, respectively. Additionally, u , v and w are the velocity components in x -, y - and z -directions, p is the static pressure, μ_{eff} is the effective dynamic viscosity of the mixture in every control volume, g is the gravitational acceleration.

The RNGk – ϵ model is used as a turbulent model for the present problem. The governing equations for the turbulent kinetic energy, k , and the dissipation rate, ϵ , are as follow:

$$\nabla \cdot (\rho k \vec{V}) = \nabla \cdot \left(\frac{\mu_t}{\sigma_k} \nabla k \right) + P_k + G_k - \rho \epsilon \quad (5)$$

$$\nabla \cdot (\rho \epsilon \vec{V}) = \nabla \cdot \left(\frac{\mu_t}{\sigma_\epsilon} \nabla \epsilon \right) + C_{1\epsilon} \frac{\epsilon}{k} P_k - C_{2\epsilon} \rho \frac{\epsilon^2}{k} + C_{3\epsilon} G_k \frac{\epsilon}{k} \quad (6)$$

where P_k is the generation of turbulent energy due to the mean velocity gradient and G_k is the generation of turbulent energy due to buoyancy. The constants of turbulent model have the following values: $\sigma_k = 1$, $\sigma_\epsilon = 1.3$, $C_{1\epsilon} = 1.44$, $C_{2\epsilon} = 1.92$, $C_{3\epsilon} = 1.3$ [36].

Energy equation:

$$\nabla \cdot (\rho C_p T \vec{V}) = \nabla \cdot (\lambda_{eff} \nabla T) + \nabla \cdot \left[\sum_{j=1}^n \frac{H_j}{M_j} (\rho_j D_{j,mix} \nabla Y_j) \right] \quad (7)$$

where C_p is the heat capacity of the humid air, λ_{eff} is the effective thermal conductivity of humid air in every control volume which depends on the turbulence model. H_j , M_j , ρ_j , $D_{j,mix}$ and Y_j are the molar specific enthalpy, molecular weight, density, diffusivity coefficient and mass fraction of species j , respectively.

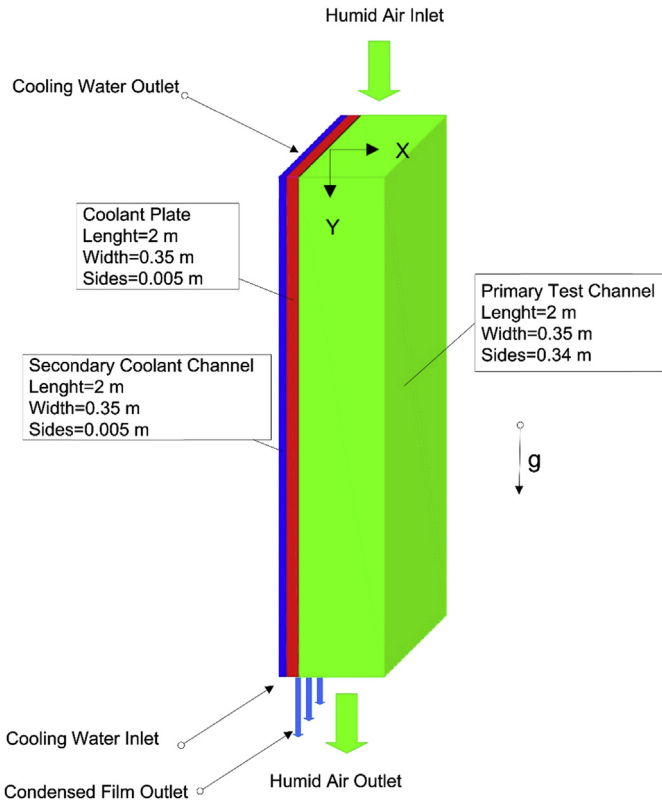


Fig. 1. The schematic view of CONAN typical classical test section.

Transport equation for non-reaction flow:

$$\nabla \cdot (\rho \vec{V} Y_j) = -\nabla \cdot \vec{J}_j + S_j \quad (8)$$

where \vec{J}_j is the diffusion flux of species j and S_j is the rate of production of species j . For every control volume, μ_t , μ_{eff} , λ_{eff} and D_{eff} could be written as Eqs. (9)–(12) and detailed in Ref. [36].

$$\mu_t = \rho C_\mu \frac{k^2}{\epsilon} \quad (9)$$

$$\mu_{eff} = \mu + \mu_t \quad (10)$$

$$\lambda_{eff} = \lambda + C_p \frac{\mu_t}{\sigma_t} \quad (11)$$

$$D_{eff} = D_{j,mix} + \frac{\mu_t}{\sigma_y} \quad (12)$$

where the mentioned constants have the following values ($C_\mu = 0.09$, $\sigma_t = 1$, $\sigma_y = 1$) [36].

Particle force balance in vector form:

$$\vec{F}_D + \vec{F}_L + \vec{F}_G + \vec{F}_P + \vec{F}_\mu + \vec{F}_B + \vec{F}_{Th} = 0 \quad (13)$$

where \vec{F}_D is the unit-mass drag force vector which is caused by the relative slip between particles and the fluid. \vec{F}_L is the shear-induced lift force vector. \vec{F}_G , \vec{F}_P and \vec{F}_μ are the buoyancy force vector, fluid pressure gradient and shear stress force vectors, respectively. \vec{F}_B stands for the stochastic excitation due to the Brownian motion and \vec{F}_{Th} represents the thermophoresis force vector. The first term of Eq. (13) is defined as in Ref. [37]:

$$\vec{F}_D = \frac{C_D Re_p}{24\zeta} (\vec{V} - \vec{V}_p) \quad (14)$$

where \vec{V}_p is particles velocity vector, $Re_p = d|U - U_p|/\nu$ is the particle Reynolds number and C_D is the drag coefficient and is given as:

$$C_D = \begin{cases} \frac{24}{Re_p} & \text{for } Re_p < 1 \\ \frac{24}{Re_p} \left(1 + \frac{1}{6} Re_p^{2/3}\right) & \text{for } 1 < Re_p < 1000 \end{cases} \quad (15)$$

In Eq. (14), ζ is the particle relaxation time defined as:

$$\zeta = \frac{sdC_c}{18\nu} \quad (16)$$

where d is the diameter of particles, ν is the humid air kinetic viscosity, s is the ratio of particles density to fluid density, C_c is the Stokes-Cunningham slip correction represented by Ref. [24]:

$$C_c = 1 + \frac{2\gamma}{d} (1.257 + 0.4e^{-1.1d/2\gamma}) \quad (17)$$

where γ is the molecular mean free path of the gas.

The second term of Eq. (13) presents the shear-induced lift force, \vec{F}_L , which is provided by Saffman [38]:

Table 1
Hydrodynamical and geometrical properties of the CONAN typical classical test section.

Thermophysical and geometrical properties		
Humid air channel	Length, (m)	2
	Width, (m)	0.35
	Side, (m)	0.34
	Inlet velocity, U_{in} (m/s)	1.5, 2, 2.5, 3, 3.5
	Inlet Pressure, P_{in} (Pa)	101,325
	Inlet temperature, T_{in} (°C)	79.13
Coolant plate (interface wall)	Inlet relative humidity, ω (%)	50, 75, 100
	Length, (m)	2
	Width, (m)	0.35
Water channel (cooling side)	Side, (m)	0.005
	Length, (m)	2
	Width, (m)	0.35
	Side, (m)	0.005
	Inlet mass flow rate, $\dot{m}_{in,w}$ (kg/s)	1.217
	Inlet temperature, $T_{in,w}$ (°C)	31.07

$$\vec{F}_L = \frac{2Kv^{0.5}\rho d_{ij}}{\rho_p d (d_{ik}d_{kl})^{0.25}} (\vec{V} - \vec{V}_p) \quad (18)$$

where $K = 2.594$ is the constant in Saffman's lift force relation and d_{ij} is the deformation rate tensor.

In Eq. (13), the buoyancy, fluid pressure gradient and shear stress forces are defined as follows:

$$\vec{F}_G = \frac{\vec{g}(\rho_p - \rho)}{\rho_p} \quad (19)$$

$$\vec{F}_p = -\frac{1}{\rho_p} \nabla P \quad (20)$$

$$\vec{F}_\mu = \frac{\mu}{\rho_p} \nabla^2 \vec{V} \quad (21)$$

The last two terms represent the stochastic excitation due to Brownian motion and the thermophoretic force is defined as follows:

$$\vec{F}_B = G_i \sqrt{\frac{216}{\pi} \frac{vk_B}{\rho d^3 s^2 C_c} \frac{T}{\Delta t}} \quad (22)$$

$$\vec{F}_{Th} = \frac{-36\mu^2 C_s (\lambda/\lambda_p + C_t + Kn)}{\rho_p \rho d^2 (1 + 3C_m Kn)(1 + 2\lambda/\lambda_p + 2C_t Kn)} \frac{\nabla T}{T} \quad (23)$$

where $C_m = 1.14$, $C_t = 2.18$ and $C_s = 1.17$ are constants and G_i and K_n are zero-mean unit variance Gaussian random number and Knudsen number, respectively.

In order to evaluate the mentioned forces and their effects on condensation of humid air, the effect of particle size can be investigated. For particles with a size of 100 nm or larger, turbulence has a larger effect than the Brownian diffusion [39]. Therefore, the Brownian force in the particle force balance can be ignored. It should be mentioned that particle deposition shows a small amount of spreading near the walls, which is due to the rather low turbulence fluctuation velocity. Meanwhile for particles with the order of 10 nm or smaller, both Brownian motion and thermophoresis are the dominant mechanisms. But variation of particle size has a lesser effect on the cited mechanism. For particles in the range of 100 nm to 4 μm , thermophoresis could be the dominant mechanism for particle deposition and for larger particles, thermophoresis is negligible. Therefore, for the investigated particle sizes in the present study ($d = 100$ nm), there is no difference in deposition rate for isothermal channel and heating/cooling channel. Although the higher temperature gradient causes the greater thermophoresis effects, for the lower temperature gradients of 10 $^\circ\text{C}/\text{cm}$, similar to the present study, particles are still affected by the thermophoresis mechanism [39].

In order to achieve a more efficient numerical scheme, we invoke several physically reasonable simplifying assumptions. Based on the related literature [10,12,23,24,40–42] the following assumptions are invoked:

- Condensation could occur only at the boundaries (cooling wall) and no condensation takes place in the form of mist or fog.
- Compared to the z-direction (normal direction), the velocity of the main flow and condensed film are much larger in the x- and y-directions.
- There is no slip condition on the surfaces.

- The multiphase system of nanoparticles and humid air is assumed incompressible along the channel and, during the condensation process, the density variation is ignored. In other words, variation of the density is only important with respect to the buoyancy effects. Therefore, the Boussinesq approximation is invoked. The other thermophysical properties of nanoparticles and humid air are assumed constant at the average temperature of the process.
- In the case of condensation, because of the difference between molecular mass of the dry air and vapor, the buoyancy force, which is caused by mass transfer and thermal diffusion, is in a downward direction. But, based on the prior description, it is not considerable.
- The gravitational force is the only external body force, which has an influence on the downward motion of the condensed film.
- The mixture enters uniformly at the inlet under an atmospheric pressure.
- In comparison with the considered domain, the condensed film is very thin and it could be assumed that, for each location along the channel, the condensed film temperature is equal to the average of interface surface and wall temperature.
- As in several studies, because of the uniform trend of the condensed film along the z-direction (normal direction), the filmwise condensation simulation is considered in 2D form.
- Volume fraction of nanoparticles is under 0.5% and the suspension is quite dilute.
- They are distributed randomly at the inlet boundary.
- There is a local thermal equilibrium between nanoparticles and main flow.
- For impingement of nanoparticles with the walls, the sticky condition is considered. Because of the low concentration of nanoparticles, this type of impingement has no considerable effect on the results.

Applying the above-cited assumptions the governing equations, i.e., continuity, momentum, energy, transport equations and the particle force balance can be written as:

Continuity:

$$\nabla \cdot \vec{V} = 0 \quad (24)$$

Momentum equations:

$$\nabla \cdot (u\vec{V}) = -\frac{1}{\rho} \frac{\partial p}{\partial x} + \frac{\mu_{eff}}{\rho} \nabla^2 u \quad (25)$$

$$\nabla \cdot (v\vec{V}) = -\frac{1}{\rho} \frac{\partial p}{\partial y} + \frac{\mu_{eff}}{\rho} \nabla^2 v + g \quad (26)$$

$$\nabla \cdot (w\vec{V}) = -\frac{1}{\rho} \frac{\partial p}{\partial z} + \frac{\mu_{eff}}{\rho} \nabla^2 w \quad (27)$$

Energy equation:

$$\nabla \cdot (T\vec{V}) = \frac{\lambda_{eff}}{\rho C_p} \nabla^2 T + \frac{1}{\rho C_p} \nabla \cdot \left[\frac{H_a}{M_a} (\rho_a D_{a,mix} \nabla Y_a) + \frac{H_v}{M_v} (\rho_v D_{v,mix} \nabla Y_v) \right] \quad (28)$$

Transport equation for non-reacting flow can be written as:

$$\nabla \cdot (\rho Y_v \vec{V}) = \nabla \cdot \left[\left(\rho D_{v,mix} + \frac{\mu_t}{Sc_t} \right) \nabla Y_v \right] \quad (29)$$

where $Sc_t = 0.7$ is the turbulence Schmidt number.

The Particle force balance can now be obtained by considering the definition of the drag force, the buoyancy force, fluid pressure gradient and shear stress force in Eqs. (14) and (19)–(21), respectively, thereby yielding:

$$\frac{3\nu C_D Re_p}{4d^2 s C_c} (\vec{V} - \vec{V}_p) + \frac{\rho_p - \rho}{\rho_p} \vec{g} - \frac{1}{\rho_p} \nabla p + \frac{\mu}{\rho_p} \nabla^2 \vec{V} + \frac{\vec{F}_{th}}{m_p} = 0 \quad (30)$$

where m_p is the mass of the particles.

Using 2d wall condensation model for the condensed film, the continuity and momentum equations could be evaluated as follows:

Continuity:

$$\nabla \cdot \vec{V}_l = 0 \quad (31)$$

Momentum equations:

$$\nabla \cdot (u_l \vec{V}_l) = -\frac{1}{\rho_l} \frac{\partial p_l}{\partial x} + \nu_l \nabla^2 u_l \quad (32)$$

$$\nabla \cdot (\nu_l \vec{V}_l) = -\frac{1}{\rho_l} \frac{\partial p_l}{\partial y} + \nu_l \nabla^2 \nu_l + g \quad (33)$$

4. Numerical implementation

Most of the CFD reports for particle transports in single-phase flow are done using a Eulerian-Lagrangian hybrid method. As it is elaborated below, the fluid phase is treated as a continuum phase using the Navier-Stokes equations, while the nanoparticles are tracked using a large number of particles through the calculated flow field.

As mentioned before, this problem consists of a convection/condensation heat transfer in a 3d domain. Additionally, discrete particles are injected into the main flow. A numerical method using a CFD commercial software was adapted for our problem. For this purpose, the species transport model in ANSYS FLUENT 15.0 was employed for wall condensation of vapor in the presence of NCG with additional nano-particles. On the basis of several previous reports [12], wall condensation plays a major role and the volume condensation is negligible. Therefore, the Eulerian wall film model is chosen as the wall condensation model. This model is only applicable for 2d thin film condensation in a 3d domain. The wall condensation process and particles distribution are executed in ANSYS FLUENT by user-defined functions (UDF). The SIMPLE algorithm is used for pressure-velocity coupling. The QUICK model is adapted for heat transfer and the Green-Gauss is used for diffusion terms. In order to insure that final solutions are converged, a maximum residual of 10^{-6} is adopted for all of the equations. The details of this method can be found in Ref. [43]. Finally, applying a Lagrangian method, the governing equation of the particle deposition is numerically solved.

4.1. Mesh properties and validation

The mesh structure of the test section is shown in Fig. 2. According to this figure, a 3d structural mesh is used. The finer mesh is performed near the coolant wall, where wall condensation occurs [44]. It is more noticeable that, the velocity gradient and temperature gradient are more visible in this area. Various ranges of grid sizes are examined to ensure that the numerical model is independent from mesh structure at different inlet conditions. Fig. 3

presents the total condensate mass flow rate at the outlet for pure saturated humid air at $U_{in} = 2.5$ m/s and $T_{in} = 80$ °C. It can be seen that for grid numbers larger than 10^6 , the variation of condensate mass flow rate is negligible. The mentioned discrepancy between condensed flow rates for different grid numbers is defined as $E_c = \left| \frac{\dot{m}_{final} - \dot{m}_i}{\dot{m}_{final}} \right| \times 100\%$ where \dot{m}_{final} and \dot{m}_i are total condensate mass flow rate at the finest mesh and the other coarser mesh size respectively. This error is also shown in Fig. 3 on the y-axis on the right side. As shown in the right hand side of this figure, repetition of the numerical calculation with finer mesh had no effect on the results. As such we had established the grid independence for our problem. Accordingly, similar comparisons were performed for various inlet conditions (i.e. inlet velocity, relative humidity and nanoparticles mass fraction) and the grid size with sufficient converged results was used. Hence, for mentioned CONAN test section, the arrangement of mesh with 10^6 grids is selected.

In order to validate the present numerical model, some of present results are compared with experimental data of Ambrosini et al. [10] and numerical results of Zschaek et al. [13] at different inlet conditions which are listed in Table 2. Fig. 4 illustrates the local surface heat flux of the cooling wall along the channel which is obtained for experiment P10-T30-V25 (without nano-particles). More details of the mentioned experimental results are listed in Ref. [11]. It is apparent from this figure that the local surface heat flux, which is predicted by the present study, is in good agreement with the experimental results. However a small discrepancy (i.e., error) exists between the results. The maximum local error is less than 13% under the same inlet conditions. This discrepancy can be due to the simplifying assumptions which are used for providing a simpler numerical model. Constant thermophysical properties at different temperature and constant density of the humid air near the interface of the condensed film are important assumptions which affect the numerical model [12]. The accuracy of the numerical model at different inlet conditions (see Table 2) is evaluated and shown in Fig. 5. The total condensate flow rate at the outlet of the channel, for various relative humidities of the pure humid air (without nano-particles), is calculated and compared with experimental data [10] and numerical results [11]. As indicated in this figure, the presented results of total condensate flow rate are in good agreement with the experimental data at different inlet velocities and relative humidities and the maximum error between the mentioned results is less than 3.8%. Therefore, Figs. 4 and 5 validate the present numerical model.

4.2. Comparison of nanoparticles materials

Using nanoparticle scan effect the thermophysical characteristic of dilute gas-particle flow and this effect can result in a higher thermal conductivity which leads to a higher condensation ratio of the humid air. However, because of the low concentration of the nano-particles, the variation of thermophysical properties is not the scope of the present study. The particle deposition effect on condensation of humid air is an important problem that is considered in the present research. As mentioned in several works in the literature, for small particles with diameters in the range from 50 nm to 1 μ m, the deposition effects of nanoparticles are more pronounced compared with the thermophysical effects [39]. Based on the particle force balance equation, see Eq. (30), for the same particles size, the variation of particle materials could be effective under variation of density and the other thermophysical properties of the nanoparticles has no effect on the condensation process. In order to evaluate the density of nano-particles, three different nano-particles, with different densities, are examined at

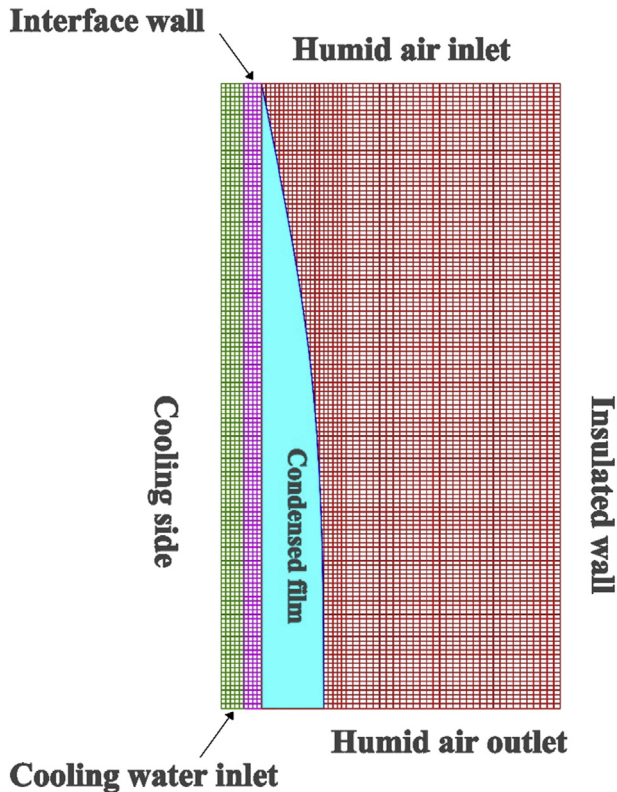


Fig. 2. 2d view of mesh sample of the CONAN test section (No scale view).

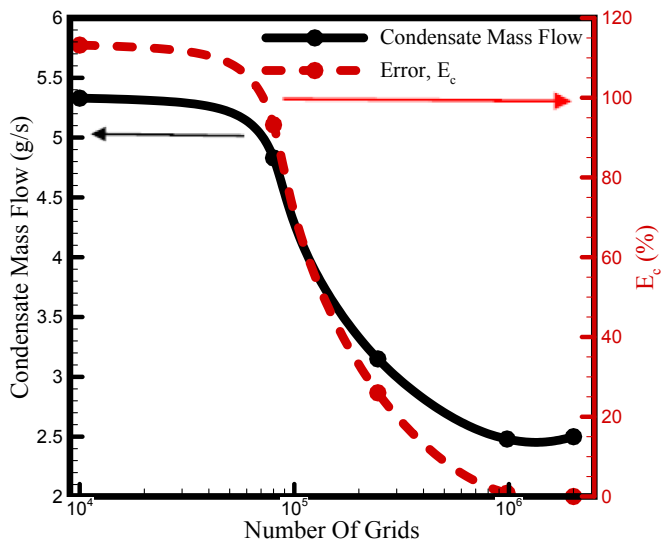


Fig. 3. Typical representation of mesh independency.

different inlet velocities and relative humidities. The thermophysical properties of these nanoparticles (copper, silicon dioxide and sodium chloride) are listed in Table 3. To compare the physical effects of these nano-particles, the local surface heat flux along the cooling wall for pure saturated humid air and the mentioned nanoparticles added at $U_{in} = 2.5$ m/s are presented in Fig. 6. As illustrated in this figure, using the nanoparticles with lower density improves the surface heat flux by 5.5%, which leads to a greater condensation ratio. As mentioned before, density and particle diameter are the only physical specifications of nanoparticles that

affect the force balance of the discrete phase. Therefore, additional silicon dioxide, sodium chloride or copper particles present the same trend. But it seems that the lower density of silicon dioxide and sodium chloride causes a little more enhancement. Whereas, nanoparticles with higher density, such as copper, have lower effect on surface heat flux. Similar comparisons are done for other inlet velocities at different relative humidities which have a similar trend. The maximum surface heat flux was verified when using sodium chloride for saturated humid air at $U_{in} = 3$ m/s. Therefore, it could be concluded that for constant particle size, $d = 100$ nm, the decrease in density of nanoparticles leads to higher surface heat flux. This trend is caused by the higher turbulent deposition losses. The investigation of different nanoparticles with similar size shows that in the highly turbulent regime, using denser nanoparticles leads to a lower deposition performance, which is equal to a lower improvement in the condensation process. In the area of convection heat transfer for turbulent flow a similar study was done by Romay et al. [45] presenting similar results.

4.3. Comparison of nanoparticles mass concentration

In order to evaluate the nanoparticles mass concentration, the Reynolds number of the condensed film at the outlet of the channel is reported for various values of relative humidity of humid air ($\phi = 100 \times$ nanoparticles mass flow rate/humid air mass flow rate = 0), and, humid air with suspended nano-particles, ($\phi = 0.5\%$ and 1%). The present comparison verified that the variation of nanoparticles mass concentration has a direct effect on the condensation of the humid air and this trend is analogous to the one verified at the investigated inlet velocities for a wide range of relative humidities, $\omega = 50$ – 100% . These results should be interpreted with caution because, as mentioned before, there are other parameters, which were assumed constant or have been ignored in the present problem. However, additional nanoparticles leads to a greater pressure drop and this effect is not very encouraging for convection heat transfer enhancement but it is significant at least in the phase change process. Accordingly, it could be concluded that condensation of the humid air in the presence of nanoparticles would be improved; nevertheless, the effect of mass concentration of nanoparticles is more considerable at higher relative humidities. At a constant inlet velocity ($U_{in} = 2.5$ m/s), for lower relative humidity ($\omega = 50\%$), additional 0.5% of nano-particle mass concentration leads to a 10.1% increase in the condensate Reynolds number. Alternatively, it can be stated that a 1% of nano-particle mass concentration causes 16.6% increase in the condensate Reynolds number. This improvement is more prominent for saturated humid air, where using nanoparticles increases the condensate Reynolds number between 21.8% and 43.6% . Comparison of condensate Reynolds number shows that, at higher relative humidities, using nanoparticles is more noticeable (see Fig. 7).

Table 2

Inlet boundary condition utilized in CONAN typical classical test section.

Experiment	Main test channel (humid air)			Secondary channel (cooling water)	
	U_{in} (m/s)	ω (%)	T_{in} ($^{\circ}$ C)	$T_{in,w}$ ($^{\circ}$ C)	$\dot{m}_{in,w}$ (kg/s)
P10-T30-V15	1.46	100	82.66	31.24	1.2171
P10-T30-V20	2.02	100	80.61	31.10	1.2173
P10-T30-V25	2.52	97.83	79.13	31.07	1.2168
P10-T30-V30	3.01	87.35	78.73	30.91	1.2160
P10-T30-V35	3.59	96.55	75.02	30.71	1.2159

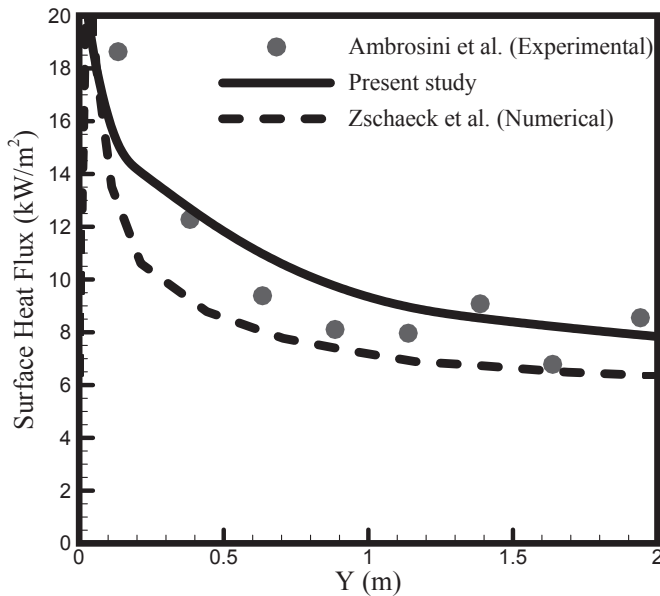


Fig. 4. Comparison of local surface heat flux between present results, experimental results by Ambrosini et al. [9] and numerical results by Zschaeck et al. [12] for experiment P10-T30-V25.

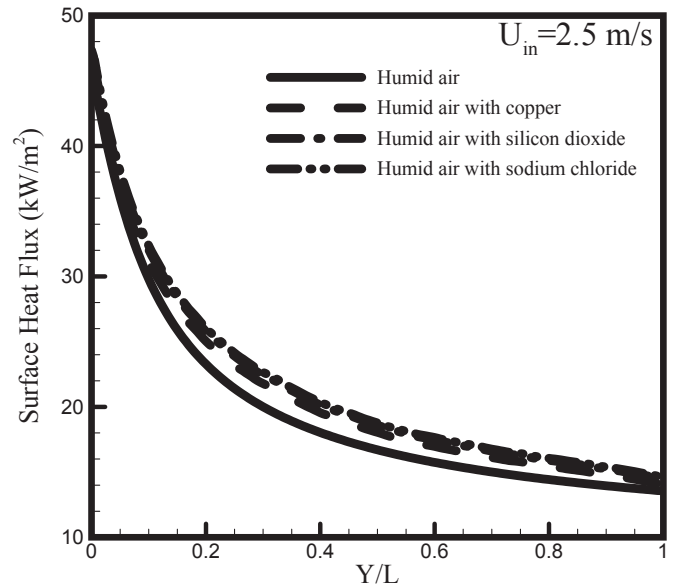


Fig. 6. Comparison of local surface heat flux for different nano-particles.

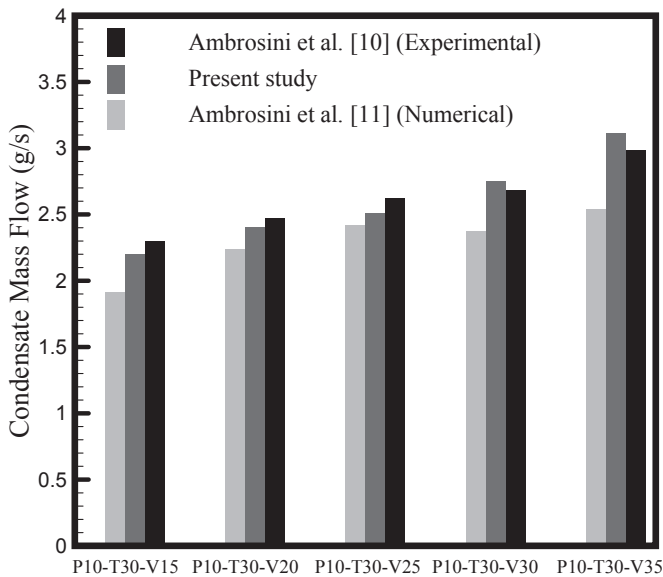


Fig. 5. Comparison of condensed mass flow at the outlet between the present results, experimental results [10] and numerical results [11] for different experiments.

Table 3
Thermophysical properties of nano-particles.

Nano-particles	Diameter (nm)	Density (kg/m ³)	Specific heat capacity (J/kg K)	Thermal conductivity (W/m K)
Copper	100	8300	420	401.0
Silicon dioxide	100	2220	745	1.38
Sodium chloride	100	2165	853	6.50

4.4. Evaluation of heat and mass transfer parameters

The influence of nanoparticles on condensation of humid air depends on inlet conditions, such as inlet velocity and relative humidity. To distinguish between these two parameters, the local

surface heat flux along the channel for various inlet velocities ($U_{in} = 1.5, 2, 2.5$ and 3 m/s) and relative humidity ($\omega = 50, 75$ and 100%) are compared in Fig. 8. As seen in this figure, the effect of nanoparticles on surface heat flux is more substantial at higher inlet velocities. Further, this improvement is more intense for saturated humid air and in the same way, the local surface heat flux increases with the rise of relative humidity in the presence of nanoparticles. Particularly, using nanoparticles can be neglected when the relative humidity is less than 50% (no noticeable increase in surface heat flux was detected). In order to assess this trend, it could be expressed that, both interaction of particle inertia and inhomogeneity of the turbulence in the channel, especially near the mass transfer interface, causes particle deposition from the more turbulent region to less turbulent regions-this is called turbophoresis [20]. Turbophoresis is due to gradient of velocities that should be considered at high Reynolds number of the main flow and has an operative effect on nanoparticle deposition. Hence, based on this mechanism, for higher inlet velocities, which translates to higher Reynolds numbers for the main flow, the stronger deposition of nanoparticles would occur that leads to an increase in mass transfer. Accordingly, for lower inlet velocities, the fluctuation of streamline is lower, so that the effect of turbophoresis would disappear. In terms of the particle force balance, these trends could be interpreted by deposition efficiency measurement which is studied by Romay et al. [45] for convection heat transfer in cooling

tube. As they observed, the deposition efficiency of NaCl particles is almost 1% for smallest particles (100 nm) and 3% for largest particles (700 nm) at $Re = 5517$. Meanwhile, corresponding deposition efficiency are 5% and 43% for smallest and largest particles at $Re = 9656$, respectively. Therefore, higher Reynolds number of the

inlet flow leads to an increase in turbulence levels, which is leading to an increase in deposition efficiency. This behavior improves both convection and condensation processes.

Using the nanoparticles influences heat and mass transfer. As such the Reynolds number for condensed film at the outlet of the channel is reported for different inlet velocities and relative humidities and compared with pure humid air for each condition (see Fig. 9). Comparison of the condensate Reynolds number for pure humid air and humid air with suspended nanoparticles ($\phi = 0.5\%$), reveals that using nanoparticles improves the mass transfer coefficient which accelerates the condensation rate. Similar to local surface heat flux, this trend is not uniform and strongly depends on the inlet velocity. For example, compared to the pure humid air case, the increase in the condensate Reynolds number is between 9.5% and 11.4% when the relative humidity increases from 50% to 100% at $U_{in} = 3$ m/s and this variation is between 2.1% and 4.8% at $U_{in} = 1.5$ m/s. As mentioned before, the absorption of nanoparticles in the condensed film is ignored. This assumption is due to ignoring the inertial impact. In other words, the strong forward movement in the turbulent regime reduces the collision of nanoparticles with the walls and the surface of the condensed film. Also, because of the low mass concentration of nanoparticles, $\phi = 0.5\%$, the absorption of nanoparticles by the condensed film is insignificant in case of a collision. Therefore, possible absorbed particles have no considerable effect on the condensed film.

Using the same conditions employed in Figs. 9 and 10 provides the results obtained for mean Nusselt number of the condensed film. The effects of nanoparticles on the mean Nusselt number, $\overline{Nu}_f = (1/L) \int Nu_f(y) dy$, for different relative humidities and inlet velocities are shown in this figure. We can deduce that using nanoparticles increases the mean Nusselt number, but the Nusselt number enhancement is not constant and depends on the inlet velocity. The maximum improvement in the Nusselt numbers is 2.6% for inlet velocity of $U_{in} = 1.5$ m/s and 4.7% for $U_{in} = 3$ m/s. There are several explanations for these results. According to the definition of the condensed Nusselt number, $Nu_f(y) = h_f(y)y/\lambda_f$, using nanoparticles causes more condensed flow which leads to a higher condensate Reynolds number, as shown in Fig. 9, and a higher

convection heat transfer coefficient in the condensed film. Therefore, a similar trend of the condensate Reynolds number could be observed for the mean Nusselt number of the condensed film.

The effects of nanoparticles on mass transfer, can be categorized through an evaluation of the Sherwood number. For humid air as a mixture of vapor and NCG, the Sherwood number represents the ratio of vapor mass transfer to the rate of diffusion and can be defined as follows [10,34]:

$$Sh(y) = \frac{y}{\rho D} \frac{\dot{m}_1''}{\log\left(\frac{Y_{n,bulk}}{Y_{n,wall}}\right)} \quad (34)$$

where \dot{m}_1'' is condensation mass flux at the interface, and Y_n is mass fraction of the air.

The local Sherwood numbers along the channel for different relative humidities at a fixed inlet velocity, $U_{in} = 3$ m/s, are compared in Fig. 11. It can be observed from this figure that the nanoparticles augments the mass flux, and this trend increases along the channel. According to prior results, the effect of nanoparticles is more significant for higher relative humidities. An increase of the turbophoresis effect along the channel results in an increase in the influence of nanoparticles. Analogous comparisons were done for various ranges of the inlet velocities in the turbulent regime and the same trends of the mentioned effects were observed. As such, using the nanoparticles could be important for a longer heat exchanger. In the other words, because of the increase of the nanoparticles fluctuation along the channel and an increase in the turbophoresis force, the mass flux of the condensate and consequently the local Sherwood number will increase.

In order to assess the influence of nanoparticles on the total mass transfer, the mean Sherwood number, $\overline{Sh} = (1/L) \int Sh(y) dy$, as a function of the relative humidity for different inlet velocities is presented in Fig. 12. The results presented in this figure display the influence of the nanoparticles on the total mass flux of vapor from the main flow to the condensed film. It can be seen that when nanoparticles are added to the main flow, there is no significant difference on the mean Sherwood number for lower inlet velocities and a clear benefit of the nanoparticles on the mass flux of the condensation could not be identified in the presented figure. For higher inlet velocities, nanoparticles enhance the mean Sherwood number between 6 and 12.3%. Based on the last two figures, it can be concluded that, for higher Reynolds number of the main flow, there is substantial evidence of improvement in the local and mean Sherwood numbers when nanoparticles were added to the main flow. As mentioned before, the mass concentration of nanoparticles was assumed constant, $\phi = 0.5\%$. It is recommended that an investigation of different nanoparticle mass concentrations and their effect on heat and mass transfer parameters to be performed in the future.

Using nanoparticles, as an enhancement method for enhancing the convective heat transfer, has been investigated in several publications in the literature especially for natural convection in closed circuit [24]. The evaluation of particle deposition effect on both convection and condensation heat transfer is the most striking result to emerge from the data. Although, the presence of nanoparticles could improve both of the mentioned heat transfer mechanisms, the assessment of these two mechanisms and finding the most effective heat transfer method, could be significant. The effect of nanoparticles on convection/condensation portions of total heat transfer, which are absorbed by the cooling wall, is shown on Fig. 13. The convection and condensation heat transfer as two main mechanisms of heat transfer of the mentioned problem are measured for different inlet velocities and relative humidities for

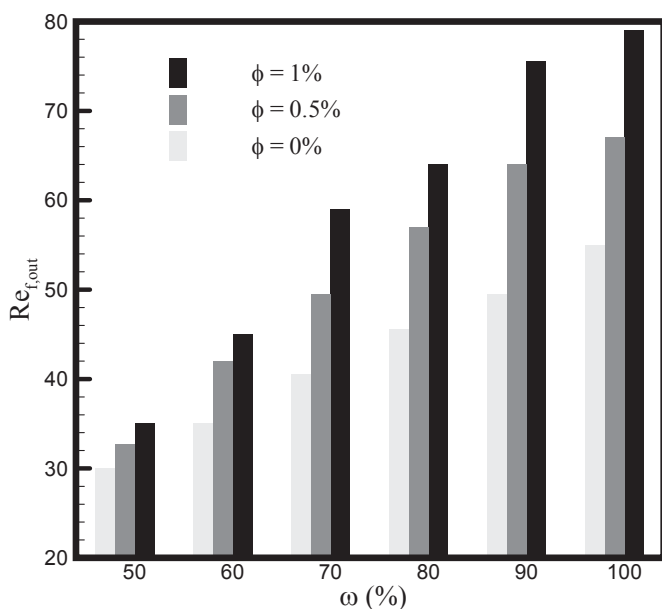


Fig. 7. The effect of mass fraction of nanoparticles on the condensed film Reynolds number at the outlet for different relative humidities at fixed inlet velocity ($U_{in} = 2.5$ m/s).

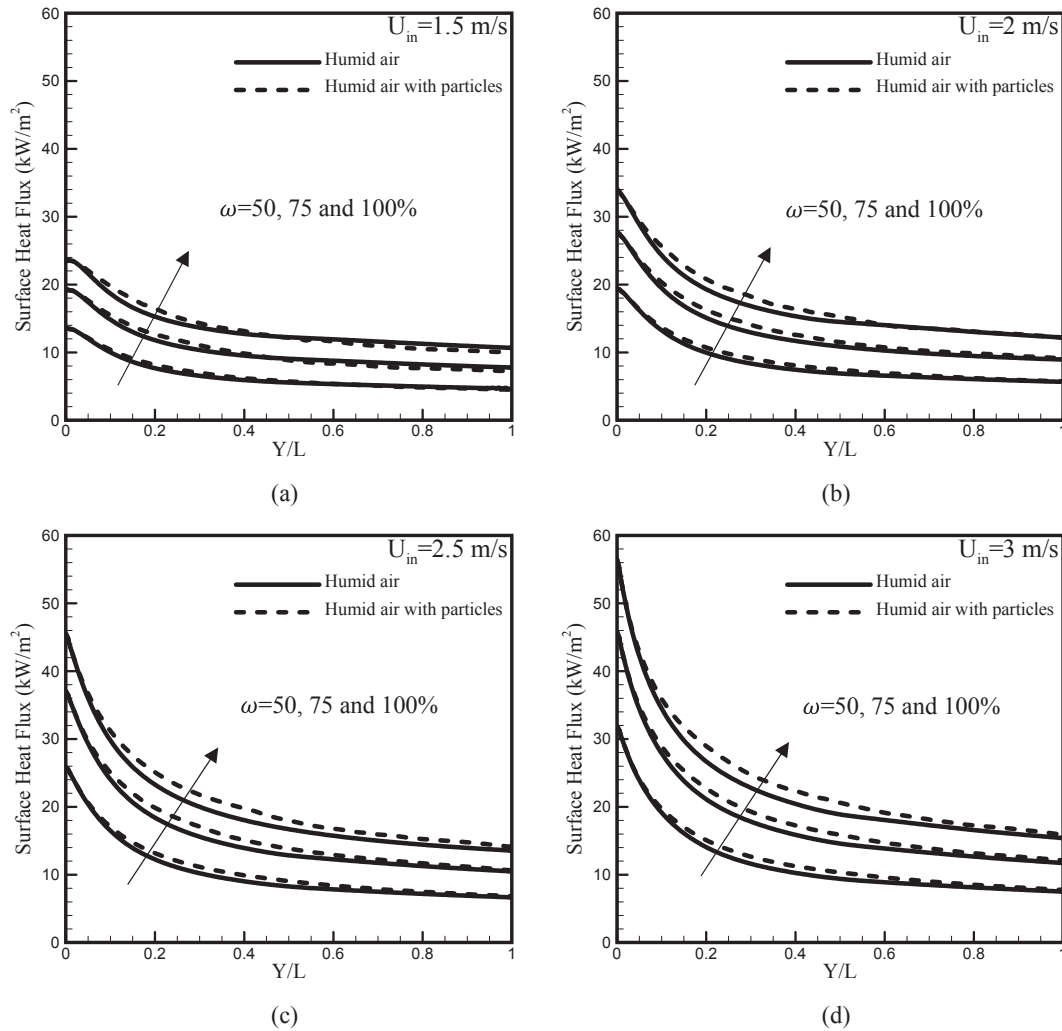


Fig. 8. Comparison of the local surface heat flux at the cooling wall between humid air and humid air with nanoparticles for different relative humidities and inlet velocities.

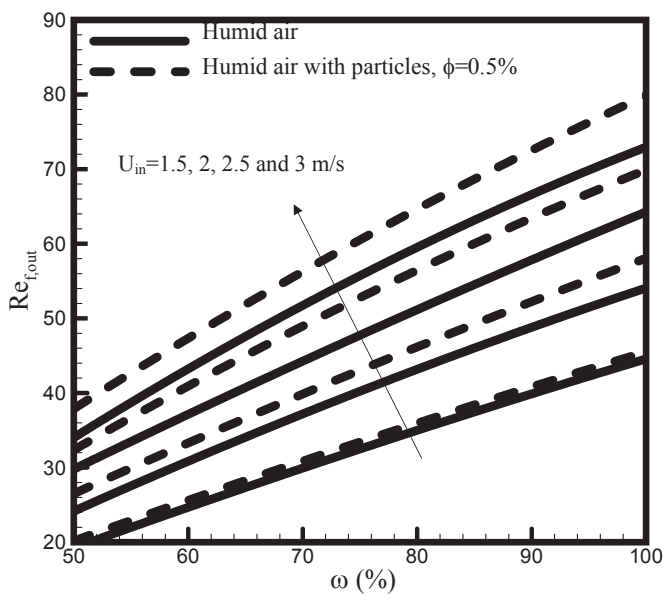


Fig. 9. Comparison of the condensed film Reynolds number at the outlet between pure humid air and humid air with nanoparticles for different relative humidities and inlet velocities.

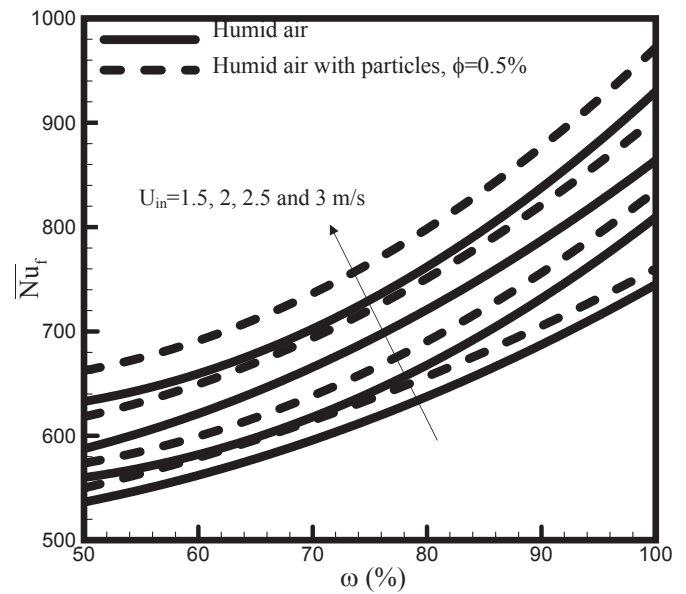


Fig. 10. The comparison of mean Nusselt number of the condensed film between pure humid air and humid air with nanoparticles for different relative humidities and inlet velocities.

both pure humid air (Fig. 13(a)) and humid air with suspended nanoparticles ($\phi = 0.5\%$, Fig. 13(b)). The comparison of these two figures shows that using nanoparticles generally increases the total heat flux. But, the improvement in the convection portion is more significant than the condensation portion. A comparison of the mentioned portions at a fixed relative humidity reveals that this improvement can possibly be more considerable for higher inlet velocities. Similarly, for a fixed inlet velocity, nanoparticles are more effective on convection portion for higher relative humidities, so that, the average improvement of the convection portion is 16.7% when nanoparticles are added to the saturated humid air, while this improvement is 10.1% for the condensation portion. Hence, nanoparticle effects on the condensation process are more limited as compared to the convection enhancement. It should be mentioned that this comparison was done for the CONAN test experiment.

The Sherwood number of the mentioned process can be compared with the Sherwood number over a flat plate where it is defined as follows [11]:

$$Sh_y = 0.0296Re_y^{0.8} Sc^{0.33} \tag{35}$$

where Sh_y , $Re_y = \rho U_{in} y / \mu$ and $Sc = \mu / \rho D$ are the local Sherwood number, the local Reynolds number and the Schmidt number, respectively. The local Sherwood number can be expressed as follows [10]:

$$Sh_y = \frac{m_i''}{\frac{M_v c D}{y} \ln \left(\frac{X_{n,bulk}}{X_{n,interface}} \right)} \tag{36}$$

where y is the distance from the inlet, m_i'' is the condensation rate at interface, c is molar concentration, M_v is molecular weight of vapor, $X_{n,bulk}$ and $X_{n,interface}$ are the molar fractions of air in the bulk and at the interface, respectively. Fig. 14 compares the mass transfer over a vertical flat plate as a function of local Reynolds number and the calculated local Sherwood number for saturated humid air and saturated humid air with suspended nanoparticles, $\omega = 100\%$ and $\phi = 0.5\%$ at constant inlet velocity, $U_{in} = 3 \text{ m/s}$. The improvement in the local Sherwood number due to additional nanoparticles is

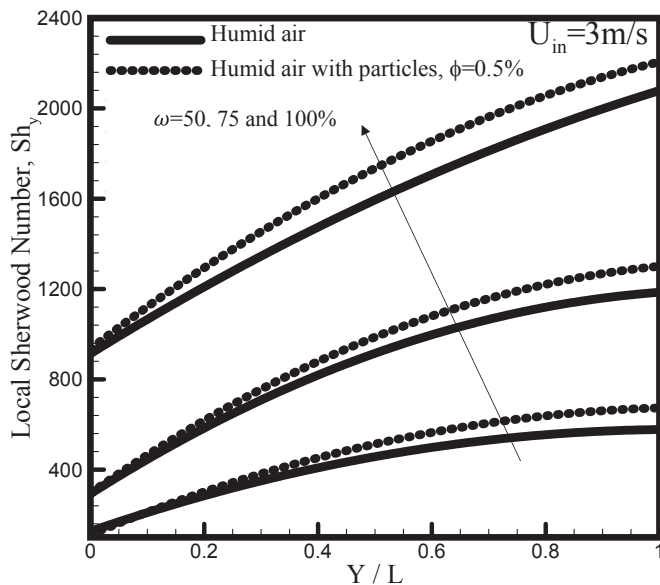


Fig. 11. The effect of nanoparticles on the local Sherwood number for different relative humidities at given inlet velocity ($U_{in} = 3 \text{ m/s}$).

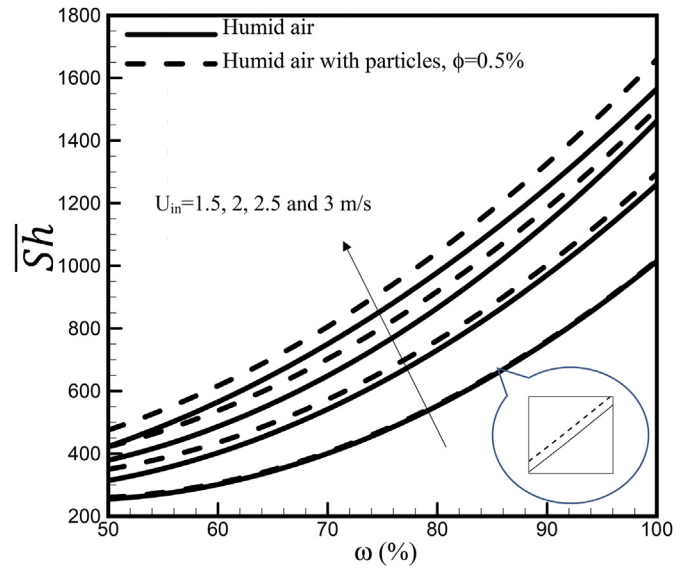


Fig. 12. Variation of the mean Sherwood number for different relative humidities and inlet velocities.

sensible along the channel. There is little discrepancy between the presented results and the mentioned correlation which is due to assumptions described earlier in this paper.

5. Response surface methodology

As mentioned before, the impact of the nanoparticles effects on heat and mass transfer enhancement is the main directive of the present study. Therefore, calculation of the perfect size of the design parameters (U_{in} , ω , ϕ), using a multi-objective function, could be an effective solution. A general multi-objective function can be presented as:

$$F(x) = [f_1(x), f_2(x), f_3(x), \dots, f_n(x)], n \geq 2 \tag{37}$$

where $x = [x_1, x_2, x_3, \dots, x_N]$ are the N design parameters and f_i are the n th objective functions. The basis of statistical methods is on allocating the single function with the special weight for each one, which is formed as follows:

$$F(x) = \min \sum_{i=0}^n \phi_i f_i(x) \tag{38}$$

where ϕ_i is the estimated weight of the single objective function. Selection and modification of the single objective's weight is the first step in finding the general effects of the nanoparticles in a wide range of the cited parameters. Also, this method is applicable in the optimization process [46]. This study uses the response surface methodology (RSM) to carry out the multi-objective function of the main process. Generally, this function is unknown and RSM can propose the suitable approximation of the multi-objective function. RSM is a group of mathematical and statistical techniques for empirical model building for design of experiments [47]. In fact, RSM estimated a response function (output variable) based on a number of simple numerical or experimental observations on an independent variable (input variable). In this method, the response function usually is formed in low-order polynomial (second order). Proposing the simple response surface, based on fewer simulation or experiments, is one of the benefits of this method [46]. It should be mentioned that RSM is one of the available statistical methods and generally, it is the best methodology. In designing an

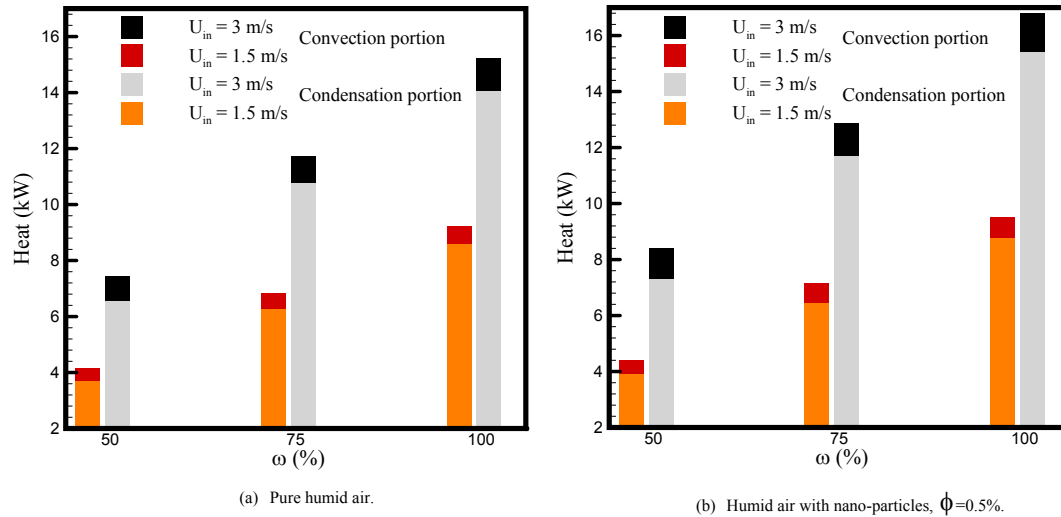


Fig. 13. Condensation/convection portion of total heat transfer for: (a) humid air and (b) humid air with nanoparticles at different relative humidities and inlet velocities.

experiment, many techniques are available and each of these techniques could be utilized for a specific problem. As such in the present condensation process, RSM is chosen. Details of the advantages of RSM can be found in Ref. [48]. Originally, RSM was developed by Box and Draper [49]. In this method several regression techniques are used to compute the weight coefficients. Choosing the regression technique and the method of data processing, are not the aim of this study and the detailed information about regression method selection and design of the numerical simulations can be found in Ref. [50].

The objective function created by RSM is formulated as:

$$F(x) = \phi_0 + \sum_{i=1}^n \phi_i x_i + \sum_{i=1}^n \sum_{j=1}^n \phi_{ij} x_i x_j + \dots \quad (39)$$

The objective functions of condensed Reynolds number at the outlet and the mean Sherwood number of the process are

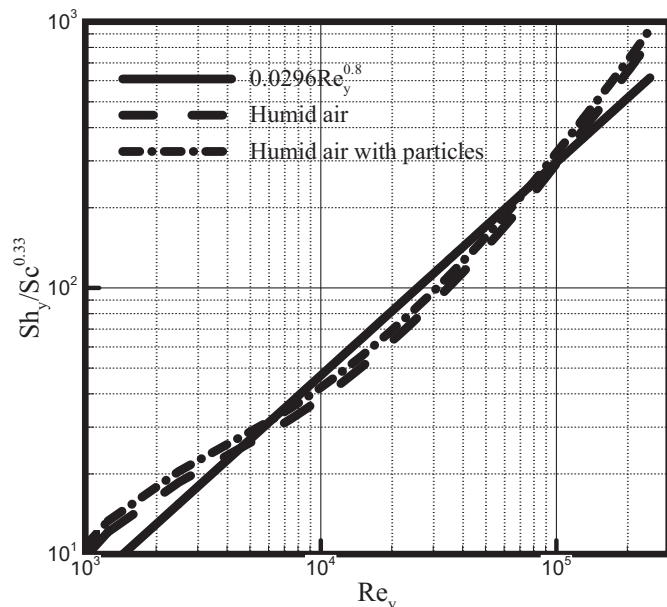


Fig. 14. Mean Sherwood number.

calculated for the range of inlet velocities from 1.5 to 3 m/s. Figs. 15 and 16 show the contour plot of the condensed Reynolds number (at the outlet) and the mean Sherwood number based on the variation of relative humidity and mass concentration of nanoparticles for $U_{in} = 2.5$ m/s. From Fig. 15, it is apparent that the nanoparticles have a uniform trend for low relative humidities as well as higher values. For the lower relative humidity, variation of condensed Reynolds number is smoother, while for higher relative humidities, this behavior is more pronounced and variation of concentration of nanoparticles has a direct effect on the enhancement of the condensation process. Consequently, the mass transfer has the same effect with respect to the variation of nanoparticles concentration, where for lower relative humidities, additional nanoparticles have a lower impact on the mean Sherwood number. However, an increase in the relative humidity, results in a more noticeable variation of the mean Sherwood number. It should be noted that even though nanoparticles improve heat and mass transfer processes; the influence of nanoparticles concentration is not substantial at lower humidities, especially when mass concentration of the nanoparticles is between 0 and 0.72%.

6. Conclusions

The objective of the present study was the systematically assess and analyze the effect of using nanoparticles on the filmwise condensation enhancement. For this purpose, the governing equations for turbulent flow and mass diffusion were modeled numerically and the condensation of humid air at different relative humidities and inlet velocities was simulated. The hydrodynamical, thermal and diffusion processes for filmwise condensation were investigated and ultimately, the following results were concluded:

- Using denser nanoparticles leads to a lower deposition efficiency and a lower turbulence level for particles, which results in an enhancement of the heat and mass transfer process.
- For all of the investigated conditions, using nanoparticles improves the condensation rate. However, the enhancement trend is not uniform for the cited conditions. The maximum observed mass transfer improvement is 12.3%.
- For low relative humidities, using nanoparticles has a lower effect on the condensation process. While, for saturated humid air, nanoparticles has a pronounced effect on the cited process.

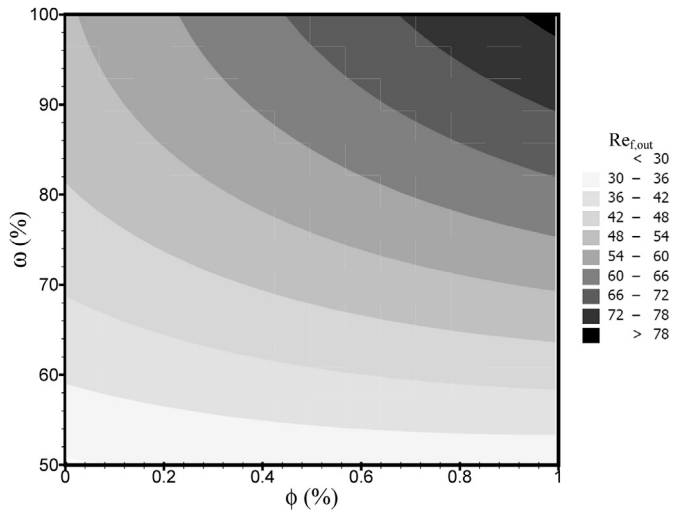


Fig. 15. Contour plot of Reynolds number of condensed film at the outlet ($U_{in} = 2.5$ m/s).

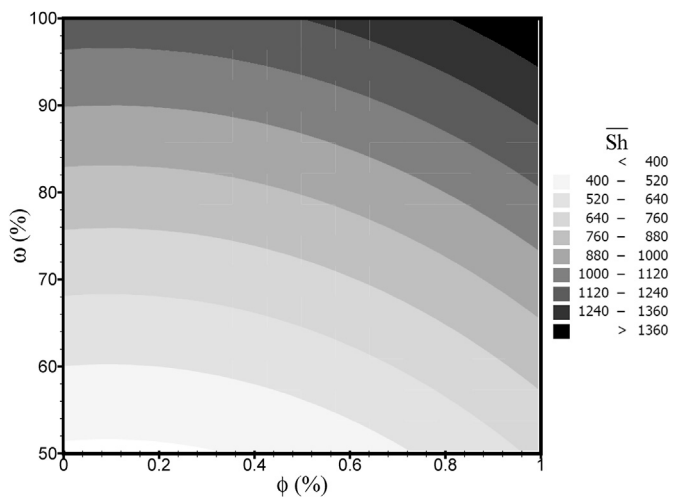


Fig. 16. Contour plot of Mean Sherwood number ($U_{in} = 2.5$ m/s).

- Concentration of nanoparticles has a significant effect on the Reynolds number of the condensed film and on the Sherwood number, where this effects is more impressive for higher relative humidities. It should be mentioned that for saturated humid air, using higher concentration of nanoparticles is more significant.

Since the application of humid air condensation is one of the most important processes for the HVAC equipments, the evaluation of the condensation process is important. Obviously, using nanoparticles enhances the heat and mass transfer processes. The above results could be useful for finding the optimum conditions for using nanoparticles to enhance the heat and mass transfer processes.

List of symbols

c	molar concentration, (mol/m^3)
C_c	Stokes-Cunningham slip correction
C_D	drag coefficient
C_p	heat capacity at constant pressure, ($\text{J}/\text{kg K}$)
d	diameter of particles, (m)
d_{ij}	deformation rate tensor

D	diffusivity coefficient, (m^2/s)
E_c	error, $E_c = \left \frac{\dot{m}_{final} - \dot{m}_i}{\dot{m}_{final}} \right \times 100\%$
\vec{F}_B	Brownian force
\vec{F}_D	drag force per unit particle mass
\vec{F}_G	Buoyancy force
\vec{F}_L	shear-induced lift force
\vec{F}_P	fluid pressure gradient force
\vec{F}_{Th}	thermophoretic force
\vec{F}_μ	shear stress force
g	gravitational acceleration, (m/s^2)
G_i	zero-mean unit variance Gaussian random number
G_k	generation of turbulent energy due to buoyancy
h	convection heat transfer coefficient, ($\text{W}/\text{m}^2 \text{K}$)
H	molar specific enthalpy, (J/kmol)
\vec{J}	vapor mass flux, ($\text{kg}/\text{m}^2 \text{s}$)
k	turbulent kinetic energy, (m^2/s^2)
Kn	Knudsen number
L	length, (m)
\dot{m}_i	total condensate mass flow rate at the primary mesh size, (kg/s)
\dot{m}_{final}	total condensate mass flow rate at the finest mesh size, (kg/s)
\dot{m}_i''	condensation mass flux, ($\text{kg}/\text{m}^2 \text{s}$)
m_p	mass of particles, (kg)
M	molecular weight, (kg/kmol)
Nu	Nusselt number
\bar{Nu}	mean Nusselt number
p	pressure, (Pa)
P_k	generation of turbulent energy due to shear
q''	local surface heat flux, (W/m^2)
Re_p	particle Reynolds number, $Re_p = d U - U_p /\nu$
s	ratio of particle density to fluid density
S	rate of production, ($\text{kg}/\text{m}^3 \text{s}$)
Sc	Schmidt number
Sh	Sherwood number
\bar{Sh}	mean Sherwood number
t	time, (s)
T	temperature, (K)
u	velocity components in x-directions, (m/s)
U	mean velocity, (m/s)
v	velocity components in y-directions, (m/s)
\vec{V}	velocity vector
w	velocity components in z-directions, (m/s)
x	Cartesian coordinate normal to cooling wall, (m)
X	molar fraction
y	Cartesian coordinate along the channel, (m)
Y	mass fraction
z	Cartesian coordinate along the width of channel, (m)

Greek symbols

ε	turbulent energy dissipation, (m^2/s^3)
ζ	particle relaxation time, (s)
γ	molecular mean free path, (m)
λ	thermal conductivity, ($\text{W}/\text{m K}$)
μ	Dynamic viscosity, (kg/ms)
ρ	density, (kg/m^3)
σ_k	turbulent Prandtl numbers for k
σ_ε	turbulent Prandtl numbers for ε
$\bar{\tau}$	stressed tensor, $\bar{\tau} = \mu \left[\left(\nabla \vec{V} + \nabla \vec{V}^T \right) - \frac{2}{3} \nabla \vec{V} \right]$
ν	kinetic viscosity, ($\text{kg}/\text{m s}$)

φ	mass concentration of nanoparticles $\varphi = 100 \times (\text{nanoparticles mass flow rate} / \text{total mass flow rate})$, (%)
ϕ	estimated weight of the single objective function
ω	relative humidity, (%)

Subscripts

a	air
ave	average
D	drag
eff	effective
exp	experimental
f	film
i	initial
in	inlet
l	interface
j	Species j
l	liquid
mix	mixture
n	noncondensable (air)
Ns	Number of parameters
p	particles
t	turbulence
Th	thermophoretic
v	vapor
w	water

References

- Ali A, Vafai K, Khaled AR. Comparative study between parallel and counter flow configurations between air and falling film desiccant in the presence of nanoparticle suspensions. *Int J Energy Res* 2003;27:725–45.
- Verma SK, Tiwari AK. Progress of nanofluid application in solar collectors: a review. *Energy Convers Manag* 2015;100:324–46.
- Webb RL, Kim N-H. *Principles of enhanced heat transfer*. New York, NY, USA: Taylor Francis; 1994.
- Amiri A, Vafai K. Analysis of dispersion effects and non-thermal equilibrium, non-Darcian, variable porosity incompressible flow through porous media. *Int J Heat Mass Transf* 1994;37:939–54.
- Caruso G, Di Maio DV. Heat and mass transfer analogy applied to condensation in the presence of noncondensable gases inside inclined tubes. *Int J Heat Mass Transf* 2014;68:401–14.
- Vafai K, Sozen M. An investigation of a latent heat storage porous bed and condensing flow through it. *J Heat Transf* 1990;112:1014–22.
- Desrayaud G, Lauriat G. Heat and mass transfer analogy for condensation of humid air in a vertical channel. *Heat Mass Transf* 2001;37:67–76.
- Rao VD, Krishna VM, Sharma K, Rao PM. Convective condensation of vapor in the presence of a non-condensable gas of high concentration in laminar flow in a vertical pipe. *Int J Heat Mass Transf* 2008;51:6090–101.
- Wu T, Vierow K. Local heat transfer measurements of steam/air mixtures in horizontal condenser tubes. *Int J Heat Mass Transf* 2006;49:2491–501.
- Ambrosini W, Bucci M, Forgione N, Oriolo F, Paci S, Magnaud J, et al. Comparison and analysis of the condensation benchmark results. In: *The 3rd European review meeting on severe accident research (ERMSAR-2008)*. Nesseber, Vigo Hotel, Bulgaria: Citeseer; 2008. p. 23–5.
- Ambrosini W, Forgione N, Merli F, Oriolo F, Paci S, Kljenak I, et al. Lesson learned from the SARNET wall condensation benchmarks. *Ann Nucl Energy* 2014;74:153–64.
- Vyskocil L, Schmid J, Macek J. CFD simulation of air–steam flow with condensation. *Nucl Eng Des* 2014;279:147–57.
- Zschaeck G, Frank T, Burns A. CFD modelling and validation of wall condensation in the presence of non-condensable gases. *Nucl Eng Des* 2014;279:137–46.
- Huang J, Zhang J, Wang L. Review of vapor condensation heat and mass transfer in the presence of non-condensable gas. *Appl Therm Eng* 2015;89:469–84.
- Saraireh M, Thorpe G. Simulation of heat and mass transfer involving vapor condensation in the presence of non-condensable gases in plane channels. In: *ASME/JSM 2011 8th thermal engineering joint conference*. American Society of Mechanical Engineers; 2011. p. T10026-T-10.
- Agrawal N, Das SK. Numerical studies on hydrogen distribution in enclosures in the presence of condensing steam. *J Heat Transf* 2015;137:121008.
- Szjártó R, Freixa J, Prasser H-M. Simulation of condensation in a closed, slightly inclined horizontal pipe with a modified RELAP5 code. *Nucl Eng Des* 2014;273:288–97.
- Sun H, Lauriat G, Nicolas X. Natural convection and wall condensation or evaporation in humid air-filled cavities subjected to wall temperature variations. *Int J Therm Sci* 2011;50:663–79.
- Hudson A. Computational analysis to enhance laminar flow convective heat transfer rate in an enclosure using aerosol nanofluids [Electronic Theses & Dissertations]. Georgia Southern University; 2013.
- Brereton G. Eulerian model for prediction of particle transport and deposition in turbulent duct flows with thermophoresis. *Aerosol Sci Technol* 2015;49:802–15.
- Walsh JK, Weimer A, Hrenya C. Thermophoretic deposition of aerosol particles in laminar tube flow with mixed convection. *J Aerosol Sci* 2006;37:715–34.
- Marti J, Haselbacher A, Steinfeld A. A numerical investigation of gas-particle suspensions as heat transfer media for high-temperature concentrated solar power. *Int J Heat Mass Transf* 2015;90:1056–70.
- Akbar M, Rahman M, Ghiaasiaan S. Particle transport in a small square enclosure in laminar natural convection. *J Aerosol Sci* 2009;40:747–61.
- Garoozi F, Shakibaeinia A, Bagheri G. Eulerian–Lagrangian modeling of solid particle behavior in a square cavity with several pairs of heaters and coolers inside. *Powder Technol* 2015;280:239–55.
- Afshar H, Shams M, Nainian S, Ahmadi G. Microchannel heat transfer and dispersion of nanoparticles in slip flow regime with constant heat flux. *Int Commun Heat Mass Transf* 2009;36:1060–6.
- Saidi M, Rismanian M, Monjezi M, Zendeabad M, Fatehiboroujeni S. Comparison between Lagrangian and Eulerian approaches in predicting motion of micron-sized particles in laminar flows. *Atmos Environ* 2014;89:199–206.
- Alam M, Hossain SC, Rahman M. Transient thermophoretic particle deposition on forced convective heat and mass transfer flow due to a rotating disk. *Ain Shams Eng J* 2015;7:441–52.
- Bertoli SL. Radiant and convective heat transfer on pneumatic transport of particles: an analytical study. *Int J Heat Mass Transf* 2000;43:2345–63.
- Bertoli SL, Valle JAB, Gerent AG, de Almeida J. Heat transfer at pneumatic particle transport—limit solutions. *Powder Technol* 2012;232:64–77.
- Guha A, Samanta S. Effect of thermophoresis on the motion of aerosol particles in natural convective flow on horizontal plates. *Int J Heat Mass Transf* 2014;68:42–50.
- Guha A, Samanta S. Effect of thermophoresis and its mathematical models on the transport and deposition of aerosol particles in natural convective flow on vertical and horizontal plates. *J Aerosol Sci* 2014;77:85–101.
- Zhang N, Zheng ZC, Glasgow L, Braley B. Simulation of particle deposition at the bottom surface in a room-scale chamber with particle injection. *Adv Powder Technol* 2010;21:256–67.
- Wang M, Lin C-H, Chen Q. Determination of particle deposition in enclosed spaces by Detached Eddy Simulation with the Lagrangian method. *Atmos Environ* 2011;45:5376–84.
- Ambrosini W, Forgione N, Manfredini A, Oriolo F. On various forms of the heat and mass transfer analogy: discussion and application to condensation experiments. *Nucl Eng Des* 2006;236:1013–27.
- Jena SK, Mahapatra SK. Numerical modeling of interaction between surface radiation and natural convection of atmospheric aerosol in presence of transverse magnetic field. *Appl Math Model* 2013;37:527–39.
- Fluent A. *12.0 theory guide*. Ansys Inc.; 2009. p. 5.
- Bagheri G, Salmandzadeh M, Golkarfarid V, Ahmadi G. Simulation of solid particles behavior in a heated cavity at high Rayleigh numbers. *Aerosol Sci Technol* 2012;46:1382–91.
- Saffman P. The lift on a small sphere in a slow shear flow. *J Fluid Mech* 1965;22:385–400.
- He C, Ahmadi G. Particle deposition with thermophoresis in laminar and turbulent duct flows. *Aerosol Sci Technol* 1998;29:525–46.
- Akbar M, Ghiaasiaan S. Radiation heat transfer and soot thermophoresis in laminar tube flow. *Numer Heat Transf Part A Appl* 2005;47:653–70.
- Faghri A, Zhang Y, Howell JR. *Advanced heat and mass transfer*. Global Digital Press; 2010.
- Laaroussi N, Lauriat G. Conjugate thermosolutal convection and condensation of humid air in cavities. *Int J Therm Sci* 2008;47:1571–86.
- Lahooti M. Navier stokes solution based on finite volume method: SIMPLE algorithm. *Isfahan University of Technology*; 2011.
- Ambrosini W, Bucci M, Forgione N, Manfredini A, Oriolo F. Experiments and modelling techniques for heat and mass transfer in light water reactors. *Science and Technology of Nuclear Installations*; 2009. p. 2009.
- Romay FJ, Takagaki SS, Pui DY, Liu BY. Thermophoretic deposition of aerosol particles in turbulent pipe flow. *J Aerosol Sci* 1998;29:943–59.
- Khuri AI, Mukhopadhyay S. *Response surface methodology*. Wiley Interdiscip Rev Comput Stat 2010;2:128–49.
- Alvarez L. Design optimization based on genetic programming. UK: Department of Civil and Environmental Engineering, University of Bradford; 2000.
- Venter G, Haftka RT, Starnes Jr JH. Construction of response surfaces for design optimization applications. In: *Proc 6-th AIAA/NASA/ISSMO symp on multidisciplinary and structural optimization*; 1996. p. 548–64.
- Box GE, Draper NR. *Empirical model-building and response surfaces*. John Wiley & Sons; 1987.
- Myers RH, Montgomery DC, Anderson-Cook CM. *Response surface methodology: process and product optimization using designed experiments*. John Wiley & Sons; 2009.